Infrared Spectroscopy of Cations in Helium Nanodroplets

*Amandeep Singh[1], Stefan Bergmeister[2], Andrew Azhagesan[3], Paul Scheier[2], and Andrey F. Vilesov[1,4]**

[1]Department of Chemistry, University of Southern California, Los Angeles, California 90089, United States

[2]Institut für Ionenphysik und Angewandte, Physik Universität Innsbruck, A-6020 Innsbruck, Austria

[3]Department of Computer Science, University of Southern California, Los Angeles, California 90089, United States

[4]Department of Physics, University of Southern California, Los Angeles, California 90089, United States

* The author to whom correspondence may be addressed: vilesov@usc.edu

Abstract

Here we describe our pulsed helium droplet apparatus for spectroscopy of molecular ions. Our approach involves the doping of the droplets of about 10 nm in diameter with precursor molecules, such as ethylene, followed by electron impact ionization. Droplets containing ions are irradiated by the pulsed infrared laser beam. Vibrational excitation of the embedded cations leads to evaporation of the helium atoms in the droplets and release of the free ions which are detected by the quadrupole mass spectrometer. In this work we upgraded the experimental setup by introducing an octupole RF collision cell downstream from the electron impact ionizer. The implementation of the RF ion guide increases the transmission efficiency of the ions. Filling of the collision cell with additional He gas leads to a decrease in the droplet size, enhancing sensitivity to the laser excitation. We show that the spectroscopic signal depends linearly on the laser pulse energy and the number of ions generated per laser pulse is about 100 times more than in our previous experiments. These improvements facilitate faster and more reproducible measurements of the spectra yielding a handy laboratory technique for spectroscopic study of diverse molecular ions and ionic clusters at low temperature (0.4 K) in He droplets.

1. Introduction

Molecular ions are important intermediates in condensed phase and atmosphere chemistry as well as in astrochemistry.[1-3] Infrared spectroscopy has been widely used for interrogation of the structure of ions as well as their reactivity and interaction with solvent species. Therefore, great strides have been made in developing new techniques for the spectroscopy of ions. Contemporary experiments often involve action spectroscopy on cold ions in molecular beams. Typically, the ions of interest are tagged with noble gas atoms or hydrogen molecules, while the absorption is tracked by dissociation of the complexes.[4-6] The tagging may cause some splitting of the bands of ionic complexes due to symmetry reduction or the presence of isomers. Recently introduced cooling in cryogenic traps filled with He gas has enabled lowering the temperature of the cations to ~ 5-10 K and tagging with weakly bound He atoms.[7-9]

Isolation in solid matrices presents another successful approach to spectroscopy of ions, [10, 11] which does not, however, offer a mass spectrometric identification desirable for the study of ionic clusters. The low temperature (~ 0.4 K), superfluid state, weak interaction, and high ionization potential of helium atoms make helium droplets an ideal matrix for spectroscopy of ions.[12-16] Observation of the ejection of molecular ions from the droplets upon infrared irradiation by M. Drabbels *et. al.*[17] has prompted further advances in the field. In the first experiments, the embedded aniline ions were produced through resonance-enhanced multiphoton ionization of the embedded molecules.[17] Alternatively, G. von Helden and co-workers produced ions through electrospray, stored them in an ion trap and then captured by the droplets.[18] Employing photoionization and electrospray techniques require a more involved apparatus as compared to the He droplet depletion spectroscopic experiment and also imposes limitations on the kinds of ions that could be produced.

Electron impact ionization (EI) presents a reliable and well-established technique for producing ions. It is long known that EI of the droplets containing few thousands of He atoms doped with neutral species leads to effective production of molecular ions and various ionic fragments.[19, 20] The ejected ions often retain several attached He atoms, giving rise to a novel way

of producing He-tagged ions for spectroscopy. This approach was recently applied in the groups of P. Scheier and A. Ellis to perform spectroscopy of $He_nC_{60}^+$ clusters, containing up to about 100 attached He atoms.[21] A. Ellis *et al.* reported the spectra of several ions tagged with up to about 20 He atoms [22-24] which were produced upon EI of the doped He droplets.

Spectroscopic study of ions through solvation in droplets of few thousand He atoms appears more favorable than through tagging by few atoms since the droplets offer a homogeneous environment with a temperature of about 0.4 K, [25] leading to narrower spectral lines. In previous works, we showed that the electron impact ionization of doped droplets is a convenient process to generate a variety of embedded ions and ionic clusters. Infrared spectra were obtained by detecting the cations released from the droplets upon laser excitation. This technique was used to study infrared spectra of several cations. [26-30] However, we also found that the infrared signal has a nonlinear laser pulse energy dependence consistent with the evaporation of the entire droplet upon multiple absorption of infrared photons.[26, 28, 29] The nonlinear dependence is inconvenient, as it leads to the requirement of high laser pulse energy on the order of 5-10 mJ and results in an ineffective detection of the weak or broad bands which have a low peak infrared absorption cross section. In addition, in the 20 cm gap between the ionizer and the laser excitation region in the experimental setup, the transmission of droplets could be affected by stray electric fields inside the chamber.[26, 28, 29] In this work we improved the transport of ions with the introduction of an octupole ion guide between the ionizer and the laser excitation region. The ion guide is mounted inside a shroud acting as a collision cell. Upon multiple collisions with additional He atoms in the collision cell, the size of the droplets containing cations decreases, providing a better response to laser excitation. As a result, we found that the spectroscopic signal depends linearly on the laser pulse energy and that the number of ions generated per laser pulse became approximately a factor of 100 larger than in our previous experiments at optimum He pressure in the collision cell. This paper describes the experimental apparatus and the tuning of the important experimental parameters.

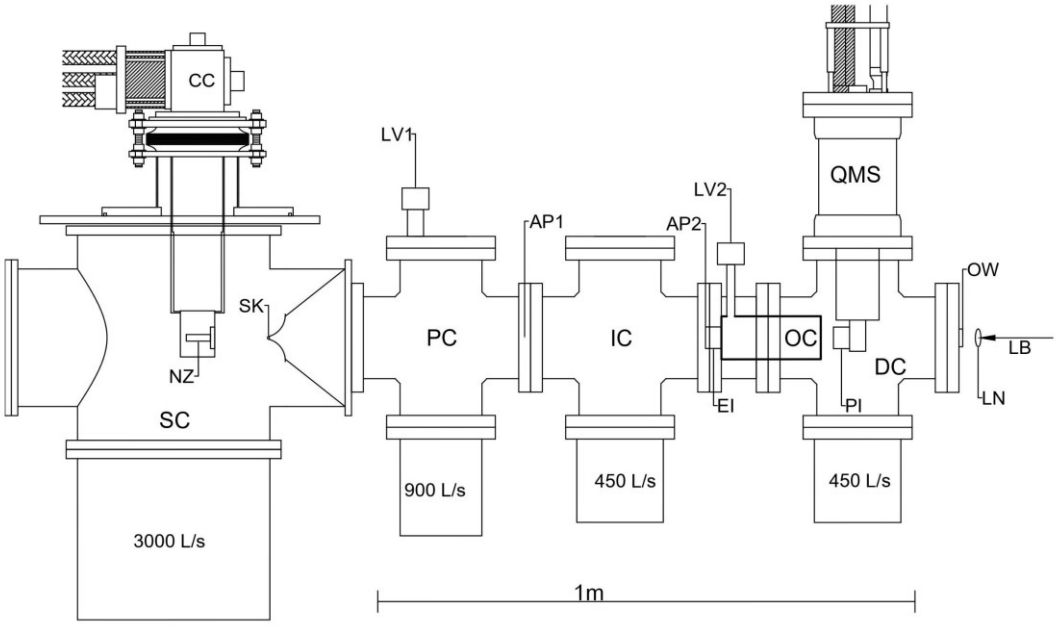

Figure 1. Schematic of the molecular beam apparatus for spectroscopy of ions in helium droplets. The drawing is approximately to scale.
SC - source chamber, PC - pickup chamber, IC - ionization chamber, DC - detection chamber, CC – cryocooler, NZ - pulsed nozzle, SK - 2 mm diameter skimmer, LV1 - leak valve for dopants, AP1- 5 mm aperture, AP2 - 5 mm aperture, EI – external electron impact ionizer, LV2 - leak valve for He gas to collision cell, OC - octupole collision cell, PI - probe ionizer, QMS-quadrupole mass spectrometer, OW - CaF_2 optical window, LN - 25 cm focal length entrance lens, LB -laser beam. Numbers show the nominal pumping speed of the turbo-molecular pumps.

2. Experimental setup

This work builds on modifications to a molecular beam UHV apparatus, which has previously been used for spectroscopy of water cations and carbo-cations.[26, 28, 29] Figure 1 shows the schematics of the experimental apparatus. The UHV apparatus is built using standard 8" UHV crosses, except for the larger custom-made source chamber (SC) which has elastomer gaskets. The pressure is measured by MKS hot cathode (series 274) ionization gauges which are not shown in Fig.1. Throughout this paper the nominal pressure is given which corresponds to the ion gauge reading without applying any gas sensitivity corrections. The apparatus employs four turbo-molecular pumps, whose pumping speed is given in the figure, which are backed by oil-free scroll

and screw pumps. Maintaining a good base vacuum on the order of low 10^{-8} - to high 10^{-9} mbar over the entire droplets beam path proved to be important to avoid the pickup of impurities, such as water and nitrogen molecules. He droplets are produced upon expansion of helium gas at a stagnation pressure of P_0 = 22 bars and a temperature of T_0 = 23 K in vacuum through a 0.5 mm diameter pulsed nozzle - NZ (General Valve series 99) attached to a Sumitomo RDK 408 cryo-cooler - CC.[31] The nozzle is controlled by a pulse driver (IOTA ONE) set to a nominal pulse width of 170-190 μs and produces pulses of He droplets of less than 100 μs in duration.[31, 32] The droplets pass through a 2 mm diameter skimmer - SK, placed about 10 cm downstream from the nozzle. Behind the skimmer, the droplets enter the 44 cm long pickup chamber - PC, where they capture dopant molecules, which were ethylene in this work. The ethylene pressure was regulated by a UHV leak valve - LV1. Further downstream, the doped droplets enter the ionization chamber - IC, that hosts an axial "external ionizer"- EI (EXTREL catalog number 812421). Ions are created by electron ionization of the He droplet beam passing through the ionizing volume. The ionizing volume is located within the ion region basket grid structure. The ionizer was typically set up to an electron energy of 100 eV and emission current of 10 mA. The ionized droplets then enter the terminal detection chamber - DC, which hosts the 22 cm long RF octupole collision cell - OC (EXTREL catalog number 815882) and the quadrupole mass spectrometer - QMS (Extrel MAX 500). The cell can be filled with He gas that is pressure regulated by a leak valve - LV2 and measured by an inline ionization pressure gauge. The OC is powered by the 2.9 MHz EXTREL QPS (Quadrupole Power Supply: EXTREL catalog number 821006). Typical pressure in different vacuum chambers is shown in Table 1.

Table 1: The nominal pressure in the different vacuum chambers of the setup measured without gases added and in the working mode (with pulsed nozzle on, ethylene added into the pickup chamber, and He gas added to the collision cell)

Chamber name	Rest gas vacuum pressure, mbar	Vacuum pressure under working conditions mbar
Source chamber	$\sim 1 \times 10^{-8}$	$\sim 1 \times 10^{-5}$
Pickup chamber	$< 3 \times 10^{-9}$	$\sim 1 \times 10^{-6}$
Ionization chamber	$<1 \times 10^{-9}$	$\sim 5 \times 10^{-7}$

Collision cell	~ 2×10^{-8}	~2×10^{-5}
Detection chamber	~ 2×10^{-9}	~1×10^{-6}

The QMS is equipped with a standard axial electron impact ionizer, which will be referred to as a probe ionizer - PI. In most of the experiments described in this paper, there was no emission current applied to the probe ionizer, while potentials were applied to the ion optics (ion region, extraction, *etc*.) as listed in table 2. In addition, the QMS could be operated in a standard mode with the probe ionizer ON (and external ionizer OFF). This mode is used in some preliminary experiments for aligning the He droplet beam, initial adjustment of the pickup pressures and determination of the flight time of the droplets from the nozzle to the QMS.

Electron impact of doped droplets in an external ionizer leads to a large variety of products, such as He_n^+, free fragment ions of the dopants, as well as dopant and fragment ions embedded in droplets.[26] The heavy droplets containing ions continue traversing towards the QMS, whereas the light ions produced post ionization are rejected by the RF octupole guide, which act as a high pass filter. In addition, the light ions are rejected due to the positive bias potential applied to the electrodes of the octupole.

The doped ionic droplets are irradiated by a pulsed infrared laser beam when they pass through the PI. The laser beam - LB is set to counter propagate with the droplet beam and is focused into the PI by a 25 cm focal length lens - LN. Upon the vibrational excitation of the ions, the energy is transferred to the droplet leading to evaporation of He atoms and to production of free ions.[26, 28, 29] The free ions are extracted, mass selected and detected by the QMS equipped with a Channeltron electron multiplier. The ion signal is amplified by a current amplifier (Stanford Research Systems, Model SR570) and recorded by a boxcar integrator (Stanford Research Systems, Model SR250) with a gate width typically set to within 3-5 μs.

The magnified schematic of the external ionizer, octupole cell and probe ionizer is shown in Fig. 2. The abbreviations are described in the caption to Fig. 2. The external ionizer and the octupole collision cell are mounted on the 8" flange between the IC and DC chambers. The external and probe ionizers are identical and have 5 mm diameter apertures. The external ionizer has an additional Einzel lens assembly (EL1-3). The octupole cell has 7.5 mm entrance and exit apertures.

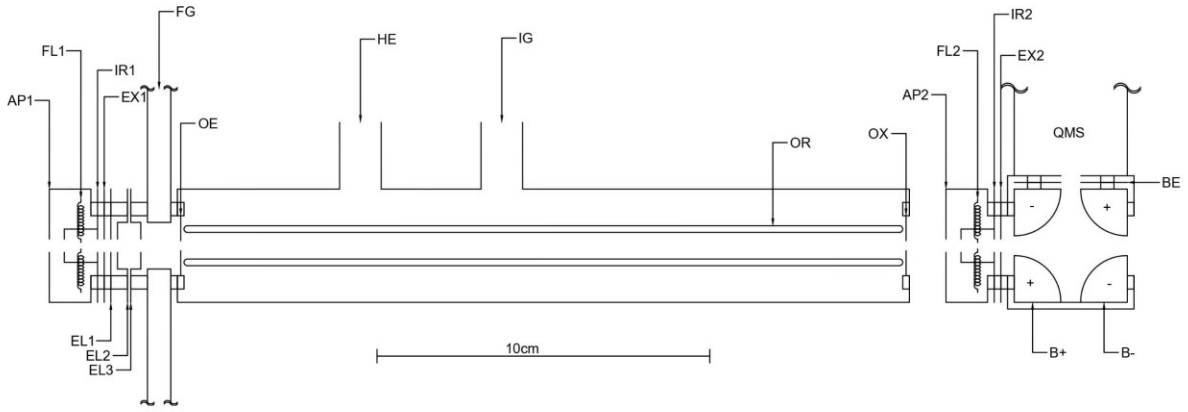

Figure 2: The close-up schematic diagram of the ionizers and octupole collision cell assembly drawn approximately to scale. The octupole cell show the simplified drawing, which only shows the component important for the discussion.
AP – aperture, FL – filaments, IR – ion region, EX – extractor, EL1-3 – Einzel lenses, FG - flange supporting external ionizer and octupole cell, OE – octupole entrance aperture, OR – octupole rods, HE- connected to helium inlet LV2, IG – connected to ion gauge, OX – octupole exit aperture, BE- bender exit aperture, B+ and B- – bender electrodes. Numbers 1 and 2 refer to the external and probe ionizers, respectively.

Table 2 shows the potentials applied to electrodes in Fig. 2 which were set to maximize the laser induced signal. Most of the potentials are floated and measured with respect to the ion region of the external ionizer - IR1. We found that most of the potentials applied to the external ionizer, octupole apertures and probe ionizer were not very critical. The potentials with respect to ground applied to the probe ionizer, bender and quadrupole are essentially the same as those in a standard QMS operation, when FL2 is used for the ionization. During spectroscopic experiments, the FL1 is on and FL2 is off. Then, IR1 is kept at 13.6 V, electron energy at 100 eV, and emission current at the maximum permissible value of 10 mA. Large ionic droplets produced upon ionization have a large kinetic energy and do not require an extraction potential, then EX1, FL1-3 and OE are equipotential with IR1. We found that the octupole bias has a large effect on the magnitude of the signal, as will be detailed in the following. The signal from smaller droplets is maximized by setting the octupole pole bias close to IR1. On the other hand, the signal from the larger droplets is higher at some potential up to 24 V with respect to IR1. The amplitude of the RF on the octupole

was set to 1000 V (corresponding to the nominal 200 amu cut off). The potential applied to AP2, which couples the octupole with the IR2, is also critical and usually set to -92 V.

Table 2. Potentials applied to electrodes in Fig. 2 during spectroscopic experiments described in this paper. All potentials are with respect to IR1 except for the IR1 itself, pole bias of the octupole and quadrupole which are with respect to ground and marked by asterisks in Table 1.

Abbreviation	Full name	Potential with respect to IR1 in Volts
AP1	Aperture 1	-100
FL1	Filament 1	-100 (I=10.0 mA)
IR1	Ion region 1	13.6*
EX1	Extractor 1	0.0
EL1	Einzel lens 1	0.0
EL2	Einzel lens 2	0.0
EL3	Einzel lens 3	0.0
OE	Octupole entrance aperture	0.0
OR	Octupole pole bias	13.6 - 38.0*
OX	Octupole exit aperture	0.0
AP2	Aperture 2	-92
FL2	Filament 2	-92 (I=0)
IR2	Ion region 2	2.0
EX2	Extractor 2	-4.0
B-	Bender	-100
B+	Bender	23
BE	Bender exit	-50
QR (not shown in Fig.2)	Quadrupole pole bias	13.5 - 38*
Channeltron	Channeltron electron multiplier	-1600*

This work employed a pulsed optical parametric oscillator-amplifier (LaserVision, with nominal spectral resolution: ~ 1 cm^{-1} unseeded, pulse duration ~ 7 ns, pulse energy ~ 5 - 8 mJ, repetition rate 20 Hz). The absolute frequency of the laser is calibrated using the photo-acoustic spectrum of methane molecules. The mid infrared output of the laser is polarized in the vertical direction. In some experiments the laser pulsed energy was attenuated using a rutile polarizer (Thorlabs GTR8_MIR rutile biprism).

The timing of the experiment is determined by the pulse generator (Quantum Composer Model 9514) which produces a sequence of pulses with a repetition rate of 20 Hz. The first pulse triggers the pulsed valve controller which produces an opening pulse for the pulsed valve typically 170-190 μs long. The trigger pulses for the Nd:YAG laser flash lamp and the Q-switch are delayed by about 2.5 - 2.9 ms. This time depends on the nozzle temperature and experimental parameters, with the goal of providing enough time for the He droplets to arrive at the IR2. The gate of the boxcar integrator is additionally delayed by about 35 μs with respect to the laser trigger pulse to allow the ions to pass through the quadrupole mass spectrometer. The trigger pulses and the signal pulses are monitored by an oscilloscope.

3. Results and Discussion

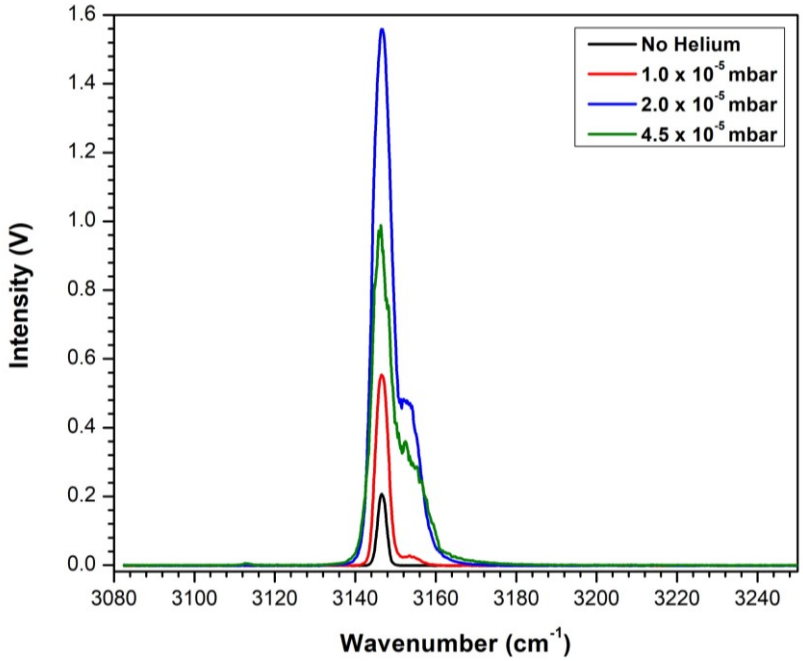

Figure 3. Infrared spectra of $C_2H_3^+$ as measured at mass channel m/z = 27 without He added to the collision cell (black) and with He added to the collision cell at different nominal pressure as indicated in the legend. The results were obtained with an amplification of 2×10^4 V/A. The nozzle operated at P = 22 bar and T = 23 K.

Throughout this work we used the infrared bands of the $C_2H_3^+$ and $C_2H_4^+$ ions, which were reported in our previous work [26] and exemplify the strong and weak signals, respectively. The ions were produced upon ionization of the He droplets doped with ethylene molecules. Figure 3 shows the spectra of the ν_6 band of $C_2H_3^+$ ions as measured at mass channel m/z = 27 without He added to the collision cell (black trace) and with He added to the collision cell at different nominal pressure as indicated in the legend. The nozzle was operated at 22 bar and 23 K. The intensity maximum was found at He pressure in the collision cell around 2×10^{-5} mbar. The spectra were recorded with an amplification of 2×10^4 V/A and at a laser pulse energy of ~6 mJ as measured at the exit of the cabinet of the OPO/OPA. The ethylene pickup pressure, laser pulse delay and the bias of the octupole were tuned to achieve the best signal as will be discussed in the following. Fig. 3 shows that at the above experimental conditions the addition of He into the collision cell

increases the intensity of the band maximum by about a factor of eight with respect to that measured without He in the cell.

To obtain the number of ions produced upon the laser pulse in the band maximum, we evaluated the integrated intensities of the signal which were recorded with the help of an oscilloscope and compared them with that for an average single ion peak. The results show that during the measurements shown in Fig. 3 each laser pulse produces ~200 ions when there is no helium in the collision cell and ~1500 ions when the cell is filled with helium added at 2×10^{-5} mbar, which corresponds to the increase of a factor of eight. The value of the increment factor strongly depends on the laser pulse energy as will be seen in Fig.7. At the same time, we did not observe any significant increase of the intensity of the baseline which may be related to some spurious ion pulses. When comparing previous measurements[26] made without the octupole RF ion guide to the current measurements where no additional He gas was added, an increase of a factor of 10 is observable. This improvement likely relates to more efficient transport of the ions from the ionizer to the laser excitation point. Considering both factors, an overall signal increase of this peak by a factor of 80 is observable.

The comparison of the traces in Fig. 3 also shows that the waveform of the spectra changes upon addition of He. The width of the band at 3146.6 cm^{-1} without He added to the collision cell is about 2 cm^{-1}, which is similar to the laser line width as estimated from the narrowest lines in the methane calibration spectrum. On the other hand, at $P_{He} = 2.1\times10^{-5}$ mbar the band width increases to about 4 cm^{-1}. The band also develops some shoulder at 3153.3 cm^{-1}, for which the relative intensity with respect to the main peak rises with He pressure. Without He added the intensity of the shoulder is very weak and can be estimated to be a factor of 1000 smaller than the main line. The broadening and appearance of the shoulder is related to the presence of He in the collision cell. At high collision pressure the spectra may reflect the excitation of the $C_2H_3^+$ solvated by the small number of He atoms. Therefore, the vibrational frequency of the $C_2H_3^+$ may become sensitive to the number of attached He atoms.[23, 24] The full understanding of this effect requires some more detailed investigation. It is seen that the spectrum with He added at pressure to achieve the maximum intensity of the spectral band, P_{MAX}, may be used to obtain some fast survey spectra. The intensity measured at $\sim2\times10^{-5}$ mbar shows linear laser pulse energy dependence as will be

shown in the following. The intensity of the band decreases and further broadening appears at higher $P_{He} = 4.5\times10^{-5}$ mbar as exemplified by the green trace in Fig.3

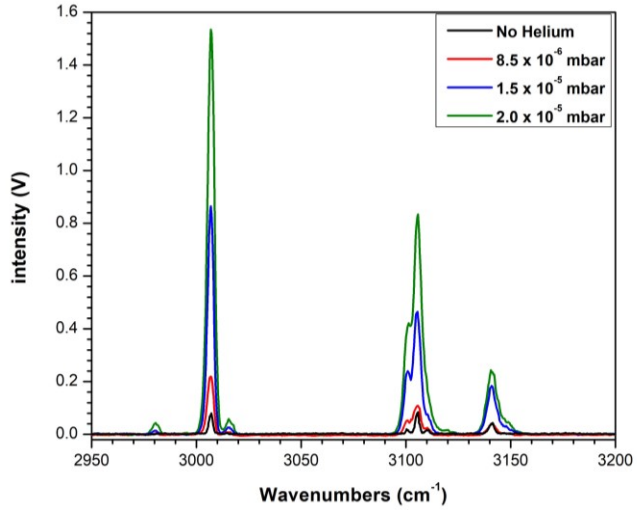

Figure 4. Infrared spectra as measured at mass channel of m/z = 28 without He added to the collision cell (black) and with He added to the collision cell at different nominal pressure as indicated in the legend. The results were obtained with an amplification of 5×10^5 V/A. The nozzle operated at 22 bar and 23 K.

Figure 4 shows the infrared spectra as measured at mass channel m/z = 28 without He added to the collision cell (black trace) and with He added to the collision cell at different nominal pressure as indicated in the legend. The spectra were measured with an amplification of 5×10^5 V/A, which is a factor of 25 higher than in Fig. 3, and at the same laser pulse energy of ~6 mJ. The two prominent bands at 3007 cm^{-1} and 3106 cm^{-1} are assigned to the ν_{11} and ν_9 bands of $C_2H_4^+$ ions, respectively.[26] The ν_9 perpendicular band at 3106 cm^{-1} measured without He shows the resolved rotational structure. The band at 3140 cm^{-1} was previously assigned to complexes of acetylene ions with hydrogen molecules ($C_2H_2^+$-H_2). [26] Fig. 4 shows that upon introduction of 2×10^{-5} mbar of He the intensity of the ν_{11} band of $C_2H_4^+$ increases by a factor of ~15, which is larger than the factor of about 8 reported for $C_2H_3^+$ in Fig. 3. This accounts for stronger nonlinear laser pulse energy dependence of the $C_2H_4^+$ bands as will be discussed in the following. Similar to the spectra of $C_2H_3^+$ in Fig. 3, the spectra of $C_2H_4^+$ in Fig. 4 at the high He pressure show broader

bands. The spectra with He also show additional weak features at 2981 cm^{-1} and 3030 cm^{-1} which remain unassigned.

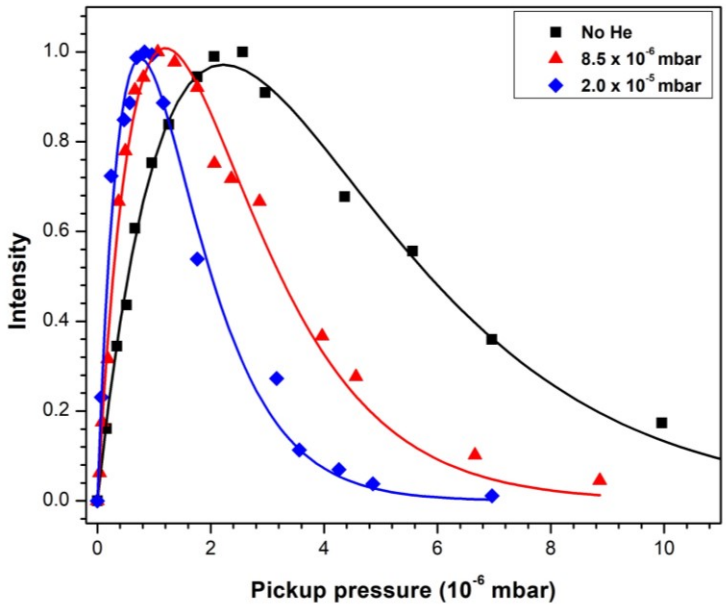

Figure 5. Nominal ethylene pickup pressure dependence of the intensity of the $C_2H_3^+$ band at 3146.6 cm^{-1}. The measurements without He added to the collision cell and at $P_{He} = 8.5\times10^{-6}$ mbar and 2.0×10^{-5} mbar in the collision cell are shown with black, red, and blue symbols, respectively. Smooth curves of same colors are fits with Poisson equation.

Fig. 5 shows the ethylene pickup pressure dependence of the intensity of the $C_2H_3^+$ band recorded with a nozzle temperature of 23 K and different helium pressure in the collision cell: without He added to the collision cell (black), and with He pressure in the collision cell of 8.5×10^{-5} mbar (red) and 2×10^{-5} mbar (blue). The data points were fitted by Poisson equation describing the probability of the capture of *k* molecules by a droplet when precursor molecules occupy the pickup chamber at the pressure - *P*:

$$I_k(P) = C \cdot \frac{(P/A)^k}{k!} e^{-P/A} \qquad (1)$$

The smooth curves in Fig. 5 are Poisson fits of the data points with $k = 1$ with A parameters obtained to be 2.2×10^{-6} mbar, 1.2×10^{-6} mbar and 0.76×10^{-6} mbar, respectively. The excellent fitting at $k = 1$ in the Poisson equation indicates that the ions are generated from the ionization of the droplets carrying a single ethylene molecule. The A value corresponds to the nominal pressure of the ethylene gas in the pickup cell when the maximum number of droplets are doped with a single ethylene molecule.

Taking the capture cross section equal to the droplets' average cross section, σ, and the average radius, R, the average number of atoms in the droplet, N, could be obtained as

$$\sigma = \frac{k_B T \cdot \alpha}{A \cdot L \cdot f_V}, \quad R = \sqrt{\frac{\sigma}{\pi}} \qquad N = \left(\frac{R}{0.224\ nm}\right)^3 \qquad (2)$$

Here k_B is the Boltzmann constant, T =295 K is the absolute room temperature, L=44 cm is the length of the pickup region, α =2.3 is the hot cathode ion gauge sensitivity factor for ethylene and

$$f_V = \sqrt{1 + \frac{v_{ethylene}^2}{v_{beam}^2}} \approx \sqrt{2} \qquad (3)$$

is the collision factor containing the root mean square velocity of the ethylene molecules of v_{ethylene} ≈ 500 m/s in the pickup chamber and the velocity of the He droplet beam of about $v_{\text{beam}} \approx$ 500 m/s. Accordingly, the average radius and the number of He atoms in the droplets responsible for the observed signal were obtained to be R = 4.6, 6.2, and 7.7 nm whereas $N = 8.6\times10^3$, 2.2×10^4, and 4.2×10^4, respectively.

A limited number of measurements were done at a nozzle temperature of 19 K and at a He nozzle pressure of 20 bar. The maximum signal for the $C_2H_3^+$ was found to be a factor of 3 higher than at 23 K and achieved at helium pressure in the collision cell of ~5×10^{-5} mbar. The measured ethylene pickup pressure dependence of the intensity similar to that in Fig. 5 showed the maximum at 4.5×10^{-7} mbar. The Poisson measurements yielded R = 10 nm and N = 9.6×10^4 for the droplets produced at 20 bar, 19 K with the pickup conditions optimized for the maximum of the signal.

Without He added, such large droplets produced very low laser induced signal. Accordingly, all of our previously published results[26, 28, 29] were obtained at the nozzle temperature of 23 K.

Even larger droplets could be produced at lower nozzle temperature,[31] which may be required to study larger cations or large ionic clusters Collision with additional He gas enables to reduce the size of the droplets which facilitates the infrared spectroscopic detection of the ions. . In spectroscopic experiments the largest practical droplet size is set by the pickup of the impurities, such as water, carbon dioxide and hydrogen. At the absolute base pressure of 10^{-8} mbar, as in the current work, the droplets containing 10^5 atoms will pick up at average 0.15 impurity molecules over the beam-pass of 1.2 m. This is undesirable, because the presence of the impurity molecules will lead to spurious bands in the spectra. Therefore, working with large droplets will require improving the baseline vacuum pressure. On the other hand, the signal drops rapidly for the nozzle temperature above 23 K, which may be specific to the pulsed nozzle arrangement we used in this work. Previous measurements[31, 32] indicated that at constant nozzle pressure, while lowering the nozzle temperature, the formation of the droplets begins abruptly at some threshold temperature and the droplets already have rather large size of few 10^4 atoms. Therefore, working at nozzle conditions of 23 K, 20 - 25 bar close to the formation threshold seems optimal for spectroscopic experiments on single ions and small ionic clusters.

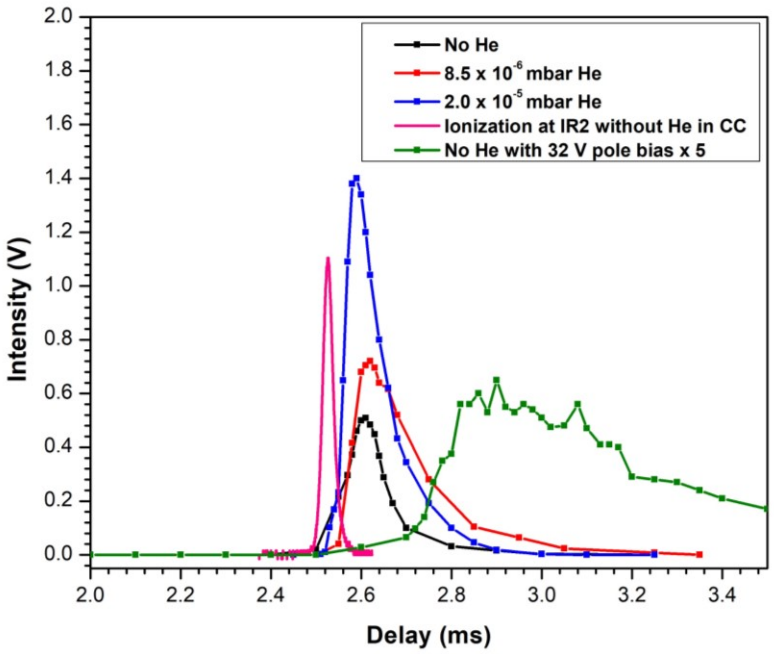

Figure 6. The dependence of the signal intensity at the $C_2H_3^+$ band maximum on the delay of the laser pulse with respect to the nozzle trigger pulse at different He gas pressure in the collision cell as indicated in the legend. The octupole pole bias was set to 15 V in black, 28 V in red, 32 V in blue and 32 V in green traces. Magenta trace shows the measurements with the droplets ionized in the IR2 with electron impact. Measurements were done for the nozzle temperature of 23 K and stagnation pressure of 20 bar. The results were obtained with an amplification of 2×10^4 V/A, except for the green trace where it was set to 2×10^6 V/A.

Figure 6 shows the intensity of the signal at the maximum of the $C_2H_3^+$ band when the laser was triggered at different delays with respect to the nozzle trigger pulse. The blue squares designate the measurements at $P_{He} = 2\times10^{-5}$ mbar, red at $P_{He} = 8.5\times10^{-6}$ mbar and black and green without He added. We found that the intensity, delay and the width of the laser-induced signals depend sensitively on the bias voltage applied to the poles of the octupole, which is given with respect to ground. The black, red and blue traces were obtained at a pole bias of 15 V, 28 V and 32 V, respectively, which were chosen to maximize the signal. The results shown by the green squares for the measurements at $P_{He} = 0$ were obtained at the octupole pole bias 32 V. The pink trace shows the measurements with the droplets ionized in the ion region 2 with electron impact, such as in a standard QMS operation. The pink trace was moved by 34 μs towards shorter times to account for

the time of flight of the ions in the QMS from the total time. From the flight time of 2.49 ms, as obtained for the maximum of the pink trace and the distance between the nozzle and the IR2 of 120 cm, the velocity of the droplets is estimated to be 482 m/s. This is in reasonable agreement with the velocity of the neutral droplets of 490 m/s estimated from the He gas enthalpy at 23 K. Some discrepancy may result from the delay of the actual nozzle pulse and the trigger pulse, which was estimated in our previous works[32] to be about 150 μs. Fig. 6 shows that the maxima of the signal obtained with laser excitation are reached at ~60-80 μs later with respect to the QMS signal (pink trace). The laser-induced signal has a width of ~100 μs as compared with ~30 μs for the QMS signal. The green trace obtained without He added and at the pole bias of 32 V has a width of about 500 μs with a sharp onset at about 2.80 ms and the center of the pulse at around 400 μs delay.

The origin of the width and delay of the signals in Fig. 6 calls for more discussion. Ideally, the width of the laser-induced signal should be the same as of the QMS signal; any broadening causes a decrease in the peak signal from the maximum possible value. Neutral droplets obtained from supersonic nozzle beam expansion have a very small velocity spread on the order of 1% of the average velocity.[32] Droplets of different size have the same velocity. For example, the droplets produced at nozzle temperature of 23 K consisting of 10^4 atoms have considerable kinetic energy of about 50 eV. Upon ionization the droplets will acquire additional kinetic energy equal to its potential applied to the ion region - IR1. If the electric potential changes along the beam path, the kinetic energy of the droplets will change accordingly, and droplets of different sizes will have different velocities. The potential applied to the poles of the octupole (pole bias) has the largest effect on the droplet travel time as indicated by the comparison of the black and green traces. Both traces were obtained without He in the cell, but with different pole biases with respect to ground of 15 V and 32 V, respectively. Application of a larger potential of 32 V leads to a large shift of the signal towards longer flight times and peak broadening. Smaller droplets must experience a larger decrease in velocity and longer delay times. The dependence at 32 V bias without He has a sharp onset at 2.8 ms, or 0.3 ms delay, with respect to the maximum for neutral droplets (pink trace). From the flight distance of 22 cm and the 0.3 ms delay the droplet size could be estimated to be about 6000 atoms. This is in reasonable agreement with the estimates in our previous works.[31, 32]

The results obtained at smaller pole bias (15 V) close to the nominal U_{IR1} = 13.6 V shows much narrower width of the signal and smaller delay times. With additional He gas in the collision cell, the optimal signal is achieved at a larger pole bias of about 30 V. With the He gas present, the signal intensities in Fig. 6 come from larger droplets which have sufficient kinetic energy to surmount the pole bias potential. Therefore, the need for the substantial bias remains unclear. Quantitative understanding of the signal may be facilitated by simulation of the ion trajectories, which is beyond the scope of this work. Such a simulation may be complicated by the unknown size distribution of the neutral droplets and unknown change of the droplet size distribution upon ionization. Collisions with He atoms in the cell will cause an additional delay and broadening of the ion signal.

We also note that using the nominal potential of the IR1 may be questionable. The QMS signal - pink trace in Fig. 6 - was obtained with a small electron current in the probe ionizer of 1 mA. We noticed that upon increase of the current to 3 mA, the peak broadens towards longer flight times. Upon further increase in the current, the intensity of the signal drops. This effect indicates that the potential of the ion region decreases significantly during the passage of the strong He droplet pulse which is caused by the buildup of the volume charge of electrons inside the ion region. This effect is stronger at larger electron currents and adds complexity to any possible simulations. Nevertheless, some estimates could be done assuming that the actual potential of the IR1 with respect to ground drops from the nominal value of 13.6 V to 8 V during the passage of the droplet pulse. Upon exit from the IR1, the droplets travel about 5 cm through the ion optics elements at 13.6 V before they enter the 22 cm long octupole with the electric potential given by the pole bias. The relevant droplets at $P_{He} = 2\times10^{-5}$ mbar, $P_{He} = 8.5\times10^{-6}$ mbar and without He added have average sizes of 4.2×10^{4}, 2.2×10^{4} and 8.6×10^{3} He atoms respectively, as estimated from the results in Fig. 5. The neutral droplets all have a velocity of 490 m/s independent of their size. Here we ignore any effect of the collisions with He gas. The delay of the ionic droplets with respect to the neutral droplet at the exit from the octupole kept at the optimal pole bias potential is calculated to be 30 μs, 51 μs and 42 μs, respectively. In comparison, if the octupole pole bias is set at 32 V, droplets containing 8600 and 6600 He atoms will experience a delay of 250 μs and 1 ms, respectively, whereas droplets smaller than 5000 He atoms will be blocked. Concerning the simplicity of the calculations, these obtained values for the delay are in reasonable agreement with the results shown in Fig.6.

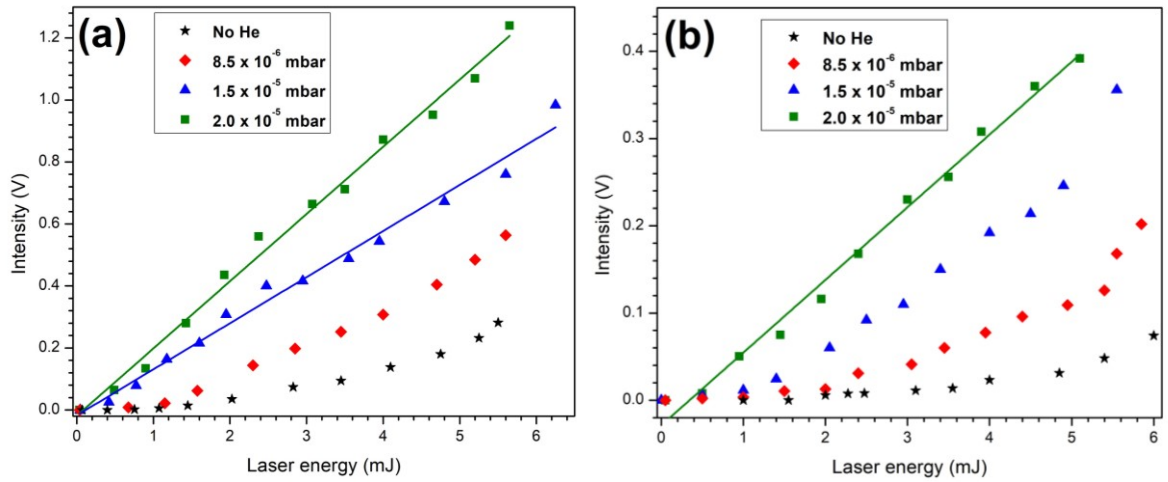

Figure 7. The dependence of the intensity of the 3146.6 cm^{-1} band of $C_2H_3^+$ (a) and of the 3006.6 cm^{-1} band of $C_2H_4^+$ (b) vs. the laser pulse energy. Black, red, blue and green traces in each panel correspond to no He added and to helium pressure in the collision cell of 0.85×10^{-5} mbar, 1.5×10^{-5} mbar, and 2×10^{-5} mbar, respectively. The results were obtained amplification of 5×10^4 V/A in (a) and 5×10^5 V/A in (b), respectively. The straight lines are linear fits to the data points.

Fig. 7 shows the dependence of the signal intensity at the maxima of the 3146.6 cm^{-1} band of $C_2H_3^+$ (a) and the 3006.6 cm^{-1} band of $C_2H_4^+$ (b) vs. the laser pulse energy at different helium pressure in the collision cell. The laser pulse energy was attenuated by the polarizer and measured close to the exit from the laser cabinet. The pulse energy at the entrance window of the vacuum apparatus is about a factor of two smaller. It is seen that the intensity obtained without He or at low He pressure have nonlinear laser pulse energy dependence. Without helium or at $P_{He} < 10^{-5}$ mbar the signal is not detectable at E< 1 mJ. Similar nonlinear dependence was observed in our previous works.[26, 28] On the other hand, the $C_2H_3^+$ signal becomes linearly dependent on the laser pulse energy in measurements with 1.5×10^{-5} mbar and 2×10^{-5} mbar He pressure in the collision cell. In comparison the weak satellite of the $C_2H_3^+$ band at 3153.3 cm^{-1} has a nonlinear laser pulse energy dependence as shown in Supplementary Materials. Some nonlinearity may remain in the $C_2H_4^+$ signal even at 2×10^{-5} mbar, which is suggested by the negative intercept of the linear fit in Fig. 7 (b). This is consistent with a larger infrared intensity of the $C_2H_3^+$ band as compared with

the $C_2H_4^+$ which were calculated to be 400 km/mol [33] and 70 km/mol [34] respectively, whereas widths of the corresponding bands are comparable, see in Fig. 3 and 4.

4. Conclusions

The results show that the introduction of the RF octupole guide between the external ionizer and the probe extractor increases the signal by about a factor of 10 in comparison to the previous measurements without the guide. This is likely related to the improved efficiency of the ion transport which may be especially important for smaller droplets, as they could be affected by some stray fields in the vacuum apparatus.

It appears that the droplets produced in the pulsed expansion have a rather broad size distribution. The distribution may have some onset on the low size, so that the fraction of the droplets smaller than the onset is very small, such as in the log-normal distribution. The laser excitation only enables the liberation of ions from droplets that contain at most 10000 helium atoms. Multiple collisions with He atoms in the cell lead to a decrease in the size of the droplets and likely creates droplets smaller than the original onset size. The liberation of the ions from these smaller droplets requires a smaller number of the absorbed photons, which explains the larger signal and more linear laser pulse energy dependence. The collision cell effectively shifts the droplet size distribution downwards, whereas the ions containing few He atoms are rejected. The combined effects of the more effective ion transport by the RF octupole and of the decreasing of the droplet size in collisions with He gas leads to a factor of 100 larger number of ions generated per laser pulse than in our previous experiments. In this work we could not estimate the size of the ionic droplets giving rise to the laser induced signal in the presence of He. The spectra obtained with He in the collision cell show considerable broadening, which may be related to the effect of the droplet size distribution in droplets containing few to few hundreds of helium atoms. Such small droplets must be produced at the very exit of the octupole, and the application of the pole bias probably serves as an extractor.

5. Supplementary Material

Supplementary Material contains laser pulse energy dependence of the main peak and satellite of the $C_2H_3^+$ band.

6. Acknowledgements

This work was supported by the National Science Foundation under Grant CHE-2102318 (A.F.V.). The authors thank Nicholas Alfonso and Kelly Yan for help during installation of the octupole cell and to Sofia Allison for carefully proofreading the manuscript. The research stay of Stefan Bergmeister at the USC was supported by the Austrian Science Fund, FWF, Project No. W1259.

References

1. N. Agmon, H. J. Bakker, R. K. Campen, R. H. Henchman, P. Pohl, S. Roke, M. Thämer and A. Hassanali, "Protons and Hydroxide Ions in Aqueous Systems," Chemical Reviews **116**, 7642-7672 (2016).
2. N. S. Shuman, D. E. Hunton and A. A. Viggiano, "Ambient and Modified Atmospheric Ion Chemistry: From Top to Bottom," Chemical Reviews **115**, 4542-4570 (2015).
3. A. G. G. M. Tielens, *The Physics and Chemistry of the Interstellar Medium*. (Cambridge University Press, Cambridge, 2005).
4. M. Okumura, L. I. Yeh, J. D. Myers and Y. T. Lee, "Infrared-Spectra of the Solvated Hydronium Ion - Vibrational Predissociation Spectroscopy of Mass-Selected $H_3O^+.(H_2O)_n.(H_2)_m$," Journal of Physical Chemistry **94**, 3416-3427 (1990).
5. J. M. Headrick, E. G. Diken, R. S. Walters, N. I. Hammer, R. A. Christie, J. Cui, E. M. Myshakin, M. A. Duncan, M. A. Johnson and K. D. Jordan, "Spectral Signatures of Hydrated Proton Vibrations in Water Clusters," Science **308**, 1765-1769 (2005).
6. O. Dopfer, "Microsolvation of the Water Cation in Argon: I. Ab Initio and Density Functional Calculations of $H_2O^+–Ar_n$ (n = 0–4)," The Journal of Physical Chemistry A **104**, 11693-11701 (2000).
7. J. Roithova, A. Gray, E. Andris, J. Jasik and D. Gerlich, "Helium Tagging Infrared Photodissociation Spectroscopy of Reactive Ions," Accounts of Chemical Research **49**, 223-230 (2016).
8. C. J. Johnson, A. B. Wolk, J. A. Fournier, E. N. Sullivan, G. H. Weddle and M. A. Johnson, "Communication: He-tagged Vibrational Spectra of the $SarGlyH^+$ and $H^+(H_2O)_{2,3}$ Ions: Quantifying Tag effects in Cryogenic Ion Vibrational Predissociation (CIVP) Spectroscopy," The Journal of Chemical Physics **140**, 221101 (2014).
9. M. Topfer, P. C. Schmid, H. Kohguchi, K. M. T. Yamada, S. Schlemmer and O. Asvany, "Infrared photodissociation of cold CH_3^+-He_2 complexes," Molecular Physics **117**, 1481-1485 (2019).
10. M. Tsuge, C.-Y. Tseng and Y.-P. Lee, "Spectroscopy of prospective interstellar ions and radicals isolated in para-hydrogen matrices," Physical Chemistry Chemical Physics **20**, 5344-5358 (2018).
11. M. E. Jacox, "The spectroscopy of molecular reaction intermediates trapped in the solid rare gases," Chemical Society Reviews **31**, 108-115 (2002).
12. R. M. P. Tanyag, C. F. Jones, C. Bernando, S. M. O. O'Connell, D. Verma and A. F. Vilesov, in *Cold chemistry: Molecular scattering and reactivity near absolute zero*, edited by O. Dulieu and A. Osterwalder (Royal Society of Chemistry, Cambridge, 2017), pp. 401-455.
13. J. P. Toennies and A. F. Vilesov, "Superfluid helium droplets: A uniquely cold nanomatrix for molecules and molecular complexes," Angewandte Chemie-International Edition **43**, 2622-2648 (2004).
14. C. Callegari and W. E. Ernst, in *Handbook of High-resolution Spectroscopy*, edited by M. Quack and F. Merkt (John Wiley & Sons, Ltd., 2011), pp. 1551.

15. M. Y. Choi, G. E. Douberly, T. M. Falconer, W. K. Lewis, C. M. Lindsay, J. M. Merritt, P. L. Stiles and R. E. Miller, "Infrared Spectroscopy of Helium Nanodroplets: Novel Methods for Physics and Chemistry," International Reviews in Physical Chemistry **25**, 15-75 (2006).
16. D. Verma, R. M. P. Tanyag, S. M. O. O'Connell and A. F. Vilesov, "Infrared spectroscopy in superfluid helium droplets," Advances in Physics-X **4**, 1553569 (2018).
17. S. Smolarek, N. B. Brauer, W. J. Buma and M. Drabbels, "IR Spectroscopy of Molecular Ions by Nonthermal Ion Ejection from Helium Nanodroplets," Journal of the American Chemical Society **132**, 14086-14091 (2010).
18. F. Bierau, P. Kupser, G. Meijer and G. von Helden, "Catching Proteins in Liquid Helium Droplets," Physical Review Letters **105**, 133402 (2010).
19. M. Lewerenz, B. Schilling and J. P. Toennies, "Successive capture and coagulation of atoms and molecules to small clusters in large liquid-helium clusters," The Journal of Chemical Physics **102**, 8191-8207 (1995).
20. A. Mauracher, O. Echt, A. M. Ellis, S. Yang, D. K. Bohme, J. Postler, A. Kaiser, S. Denifl and P. Scheier, "Cold physics and chemistry: Collisions, ionization and reactions inside helium nanodroplets close to zero K," Physics Reports-Review Section of Physics Letters **751**, 1-90 (2018).
21. M. Kuhn, M. Renzler, J. Postler, S. Ralser, S. Spieler, M. Simpson, H. Linnartz, A. G. G. M. Tielens, J. Cami, A. Mauracher, Y. Wang, M. Alcami, F. Martin, M. K. Beyer, R. Wester, A. Lindinger and P. Scheier, "Atomically Resolved Phase Transition of Fullerene Cations Solvated in Helium Droplets," Nature Communications **7**, 13550 (2016).
22. J. A. Davies, N. A. Besley, S. F. Yang and A. M. Ellis, "Probing Elusive Cations: Infrared Spectroscopy of Protonated Acetic Acid," The Journal of Physical Chemistry Letters **10**, 2108-2112 (2019).
23. J. A. Davies, N. A. Besley, S. Yang and A. M. Ellis, "Infrared spectroscopy of a small ion solvated by helium: OH stretching region of He_N–$HOCO^+$," The Journal of Chemical Physics **151**, 194307 (2019).
24. J. A. Davies, C. Schran, F. Brieuc, D. Marx and A. M. Ellis, "Onset of rotational decoupling for a molecular ion solvated in helium: From tags to rings and shells," Physical Review Letters **130**, 083001 (2023).
25. M. Hartmann, R. E. Miller, J. P. Toennies and A. Vilesov, "Rotationally Resolved Spectroscopy of SF_6 in Liquid-Helium Clusters - a Molecular Probe of Cluster Temperature," Physical Review Letters **75**, 1566-1569 (1995).
26. S. Erukala, A. J. Feinberg, A. Singh and A. F. Vilesov, "Infrared spectroscopy of carbocations upon electron ionization of ethylene in helium nanodroplets," The Journal of Chemical Physics **155**, 084306 (2021).
27. S. Erukala, A. J. Feinberg, C. J. Moon, M. Y. Choi and A. F. Vilesov, "Infrared spectroscopy of ions and ionic clusters upon ionization of ethane in helium droplets," The Journal of Chemical Physics **156**, 204306 (2022).
28. D. Verma, S. Erukala and A. F. Vilesov, "Infrared Spectroscopy of Water and Zundel Cations in Helium Nanodroplets," The Journal of Physical Chemistry A **124**, 6207-6213 (2020).
29. S. Erukala, D. Verma and A. F. Vilesov, "Rotation of CH_3^+ cations in helium droplets," The Journal of Physical Chemistry Letters **12**, 5105-5109 (2021).

30. C. J. Moon, S. Erukala, A. Feinberg, A. Singh, M. Y. Choi and A. F. Vilesov, "Formation of the $C_4H_n^+$ (n=2–5) ions upon ionization of acetylene clusters in helium droplets " The Journal of Chemical Physics **158**, https://doi.org/10.1063/1065.0150700 (2023).
31. D. Verma and A. F. Vilesov, "Pulsed helium droplet beams," Chemical Physics Letters **694**, 129-134 (2018).
32. M. N. Slipchenko, S. Kuma, T. Momose and A. F. Vilesov, "Intense pulsed helium droplet beams," Review of Scientific Instruments **73**, 3600-3605 (2002).
33. G. E. Douberly, A. M. Ricks, B. W. Ticknor, W. C. McKee, P. v. R. Schleyer and M. A. Duncan, "Infrared photodissociation spectroscopy of protonated acetylene and its clusters," The Journal of Physical Chemistry A **112**, 1897-1906 (2008).
34. S.-C. Chen, M.-C. Liu, T.-P. Huang, C.-H. Chin and Y.-J. Wu, "Photodissociation and infrared spectra of ethylene cations in solid argon," Chemical Physics Letters **630**, 96-100 (2015).